Subspace-based and single dataset methods for STAP in heterogeneous environments

Jean-François Degurse[1,2], **Sylvie Marcos**[2], **Laurent Savy**[1]

[1]Electromagnetism and Radar Department, ONERA
Palaiseau, France

[2]L2S, Univ.ParisSud11-CNRS-SUPELEC
Gif-sur-Yvette, France

email : jean-francois.degurse@onera.fr, marcos@lss.supelec.fr, lsavy@onera.fr

Keywords: STAP, single dataset, heterogeneous clutter

Abstract

Heterogeneous situations are a serious problem for Space-Time Adaptive Processing (STAP) in an airborne radar context. Indeed, traditional STAP detectors need secondary training data that have to be target free and homogeneous with the tested data. Hence the performances of these detectors are severely impacted when facing a heavily heterogeneous environment. Single dataset algorithms such as APES have proved their efficiency to overcome this problem by only using primary data. However, restricting the estimation domain to the sole primary data often implies a bad estimation of the covariance matrix which can cause a performance degradation. We here investigate the use of reduced-rank STAP on the single dataset APES method.

1 Introduction

STAP performs two-dimensional space and time adaptive filtering where different space channels are combined at different times [10]. In the context of radar signal processing, the aim of STAP is to remove ground clutter returns, in order to enhance slow moving target detection. Filter's weights are adaptively estimated from training data in the neighborhood of the range cell of interest, called cell under test (CUT). The estimation of these weights is always deducted, more or less directly, from an estimation of the covariance matrix of the received signal, which is the key quantity in the process of adaptation [9]. Any implementation of STAP processing must remain absolutely consistent with the strategy of radar processing which purpose is to obtain a high probability of detection while maintaining a very low probability of false alarm.

Classical space-time adaptive processing (STAP) detectors are strongly limited when facing a severe non stationary environment (heterogeneous clutter or a high target density). Indeed in this case representative target free training data are no longer available. To overcome this problem, the Maximum Likelihood Estimation Detector (MLED) [2] only operates with the data in the cell under test so that its performance is no longer impacted by nonstationarity. On the other side, restricting the data sample to the primary data lowers the number of data to estimate the covariance matrix which can cause a performance degradation. In this paper, we will show that implementing a subspace-based approach in conjunction with the Amplitude and Phase Estimation (APES) [11] improves the MLED detector when a target is present in the data under test. Moreover, we will then present a fast implementation of the subspace-based approach which allows a reduced computational complexity load. Section 2 is devoted to the data model, and section 3 summarizes the principle of the MLED APES-based detector. The proposed APES-based subspace methods are presented in section 4. First, the principle of the eigencanceller-based (EC) APES is derived. Secondly, a fast implementation of the subspace-based MLED detector is proposed via a pulse-recursive algorithm. In section 5, simulations are given to show that the proposed approach outperforms the MLED algorithm while reducing the computational load and the convergence time.

2 Data model

Consider a radar antenna made of N sensors that acquires M_p pulse snapshots for each l range gate. We will only use the primary data so we will forget the range gate dimension, also called fast-time dimension. Then the processing algorithm works independently in each range cell. We adopt the following two hypothesis model where H_0 and H_1 means that no target or a target is present, respectively :

$$H_0 : \mathbf{X} = \mathbf{N} \tag{1}$$

$$H_1 : \mathbf{X} = \alpha \mathbf{s_s} \mathbf{s_t}^{\mathbf{T}} + \mathbf{N} \tag{2}$$

where the received data have been arranged into an $M \times K_t$ matrix $\mathbf{X}$ with K_t being the number of training data snapshots, M the number of pulses of the spatio-temoporal vector, α the complex amplitude. $\mathbf{s_s}$ is the spatio-temporal steering vector (length NM), $\mathbf{s_t}$ the temporal steering vector (length $K_t = M_p - M + 1$) and $\mathbf{N}$ is the interference (clutter plus noise) matrix.

The covariance matrix $\mathbf{R}$ is estimated from $\mathbf{X}$ as follows :

$$\mathbf{R} = \frac{\mathbf{1}}{\mathbf{K_t}} \mathbf{X}\mathbf{X}^{\mathbf{H}} \tag{3}$$

Classical STAP detectors use the Sample Matrix Inversion (SMI) [10][9] algorithm to perform target detection from the output SNIR power :

$$\mathbf{P}_{SMI} = \frac{|\mathbf{s_s^H R^{-1} x}|^{\mathbf{2}}}{\mathbf{s_s^H R^{-1} s_s}} \underset{H_1}{\overset{H_0}{\lessgtr}} \eta \tag{4}$$

3 The Maximum likelihood Estimation Detector

3.1 Description of the detector

The MLED detector [1] takes advantage of the APES [11] algorithm in order to remove the signal of interest from the covariance matrix. The problem is stated as follows :

$$\min_{w,\alpha} (\mathbf{w^H X} - \alpha \mathbf{s_t}^T)(\mathbf{w^H X} - \alpha \mathbf{s_t}^T)^H \text{ s.t } \mathbf{w}^H \mathbf{s}_s = 1 \tag{5}$$

The obtained solution is :

$$\mathbf{w} = \frac{\mathbf{Q}^{-1}\mathbf{s}_s}{\mathbf{s}_s^H \mathbf{Q}^{-1} \mathbf{s}_s} \text{ and } \alpha = \frac{\mathbf{w}^H \mathbf{X} \mathbf{s}_t^*}{K_t} \tag{6}$$

where

$$\mathbf{Q} = \mathbf{R} - \mathbf{g}\mathbf{g^H}, \mathbf{g} = \frac{\mathbf{X s_t^*}}{\mathbf{K_t}} \tag{7}$$

Detection is achieved using the SINR output power:

$$\mathbf{P}_{MLED} = \frac{|\mathbf{s_s^H Q^{-1} g}|^{\mathbf{2}}}{\mathbf{s_s^H Q^{-1} s_s}} \underset{H_1}{\overset{H_0}{\lessgtr}} \eta \tag{8}$$

As mentioned before, the number of data samples used for the covariance matrix estimation in (3) used in (7) is equal to K_t whereas the data vector size is NM. To achieve good performance, K_t has to be larger or at least equal to $2MN$ to meet Reed's rule [6]. In an operational situation, however, this condition is difficult to satisfy. We will show in subsections *C* and *D* how subspace based methods applied together with the APES algorithm can overcome this problem. For this, we first analyse the APES algorithm through (6)-(7).

3.2 Development of the MLED method

In order to explore the use of subspace-based methods, we have to go deeper in the formulation of the APES algorithm. Indeed, these methods will only work if the clutter subspace of the covariance matrix $\mathbf{R}$ remains very close to the clutter subspace of the target free covariance matrix $\mathbf{Q}$. For a given distance cell, if there is no target at this range, the covariance matrix $\mathbf{R}$ only contains interference, i.e clutter and possibly jamming signal, and noise, according to (3) :

$$\mathbf{R} = \frac{\mathbf{X}\mathbf{X}^{\mathbf{H}}}{K_t} = \frac{\mathbf{N}\mathbf{N}^{\mathbf{H}}}{K_t} \tag{9}$$

The eigenvalue decomposition of $\mathbf{R}$ allows us to dissociate the interference subspace from the noise subspace. However, if a target is present at this range gate, it is no longer possible to isolate the interference subspace because the target is part of the dominant subspace [1]. Indeed, in this case, the covariance matrix $\mathbf{R}$ can be written using the data model defined in (2) with $\mathbf{s_{t(t)}}$ being the temporal steering vector of the target:

$$\mathbf{R} = \frac{\mathbf{X}\mathbf{X}^{\mathbf{H}}}{K_t} = \frac{(\alpha \mathbf{s_s} \mathbf{s_{t(t)}^T} + \mathbf{N})(\alpha \mathbf{s_s} \mathbf{s_{t(t)}^T} + \mathbf{N})^{\mathbf{H}}}{K_t} \tag{10}$$

$$\mathbf{R} = \mid \alpha \mid^2 \mathbf{s_s} \mathbf{s_s^H} + \frac{\alpha \mathbf{s_s} \mathbf{s_{t(t)}^T} \mathbf{N}^{\mathbf{H}}}{K_t} + \frac{\alpha^* \mathbf{N} \mathbf{s_{t(t)}^*} \mathbf{s_s^H}}{K_t} + \frac{\mathbf{N}\mathbf{N}^{\mathbf{H}}}{K_t} \tag{11}$$

If α and $\mathbf{N}$ are not correlated and the number of estimates K_t is high, (11) can be approximated to:

$$\mathbf{R} \approx \mid \alpha \mid^2 \mathbf{s_s} \mathbf{s_s^H} + \frac{\mathbf{N}\mathbf{N}^{\mathbf{H}}}{K_t} \neq \frac{\mathbf{N}\mathbf{N}^{\mathbf{H}}}{K_t} \tag{12}$$

The result of (12) indicates that the covariance matrix $\mathbf{R}$ contains interference and target signal, so if we use it as in the classical SMI method (4), we will remove both the interference and the target. According to (7) :

$$\mathbf{g}\mathbf{g}^{\mathbf{H}} = \frac{\mathbf{X} \mathbf{s_{t(D)}^*} \mathbf{s_{t(D)}^T} \mathbf{X}^{\mathbf{H}}}{K_t^2} \tag{13}$$

with $\mathbf{s_{t(D)}}$ being the temporal steering vector of the Doppler cell under test. Using the data model (2), we can write:

$$\mathbf{g}\mathbf{g}^{\mathbf{H}} = \frac{(\alpha \mathbf{s_s} \mathbf{s_{t(t)}^T} + \mathbf{N}) \mathbf{s_{t(D)}^*} \mathbf{s_{t(D)}^T} (\alpha \mathbf{s_s} \mathbf{s_{t(t)}}^{\mathbf{T}} + \mathbf{N})^{\mathbf{H}}}{K_t^2} \tag{14}$$

Using the same approximation than in (12), 14 leads to:

$$\mathbf{g}\mathbf{g}^{\mathbf{H}} \approx \frac{\mid \alpha \mid^2 \mathbf{s_s} \mathbf{s_{t(t)}^T} \mathbf{s_{t(D)}^*} \mathbf{s_{t(D)}^T} \mathbf{s_{t(t)}^*} \mathbf{s_s^H} + \mathbf{N} \mathbf{s_t^*} \mathbf{s_{t(D)}^T} \mathbf{N}^{\mathbf{H}}}{K_t^2} \tag{15}$$

Let us note

$$\rho = \mathbf{s_{t(t)}^T} \mathbf{s_{t(D)}^*} \mathbf{s_{t(D)}^T} \mathbf{s_{t(t)}^*} = \mid \mathbf{s_{t(t)}^T} \mathbf{s_{t(D)}^*} \mid^{\mathbf{2}} \tag{16}$$

The modified covariance matrix $\mathbf{Q}$ in (7) then becomes :

$$\mathbf{Q} \approx (1 - \frac{\rho}{K_t^2}) \mid \alpha \mid^2 \mathbf{s_s} \mathbf{s_s^H} + \frac{\mathbf{N}\mathbf{N}^{\mathbf{H}}}{K_t} - \frac{\mathbf{N} \mathbf{s_t^*} \mathbf{s_t^T} \mathbf{N}^{\mathbf{H}}}{K_t^2} \tag{17}$$

When testing the Doppler cell of the target, i.e $\mathbf{s_{t(D)}} = \mathbf{s_{t(t)}} = \mathbf{s_t}$, $\rho = K_t^2$, (14) becomes :

$$\mathbf{g}\mathbf{g}^H = \frac{(\alpha \mathbf{s_s} \mathbf{s_t}^T \mathbf{s_t^*} + \mathbf{N} \mathbf{s_t^*})(\alpha^* \mathbf{s_t^T} \mathbf{s_s^H} + \mathbf{s_t^T} \mathbf{N}^{\mathbf{H}})}{K_t^2} \tag{18}$$

and then

$$\mathbf{g}\mathbf{g}^{\mathbf{H}} = \mid \alpha \mid^2 \mathbf{s_s} \mathbf{s_s^H} + \frac{\alpha \mathbf{s}_s \mathbf{s}_t^T \mathbf{N}^{\mathbf{H}}}{K_t} + \frac{\alpha^* \mathbf{N} \mathbf{s_t^*} \mathbf{s_s^H}}{K_t} + \frac{\mathbf{N} \mathbf{s_t^*} \mathbf{s_t^T} \mathbf{N}^{\mathbf{H}}}{K_t^2} \tag{19}$$

[1] The dominant subspace is spanned by the eigenvectors associated with the eigenvalues higher than the noise variance

Hence from (11), (7) and (19), matrix $\mathbf{Q}$ is, without approximation :

$$\mathbf{Q} = \frac{\mathbf{N}\mathbf{N}^{\mathbf{H}}}{K_t} - \frac{\mathbf{N}\mathbf{s}_{\mathbf{t}}^{*}\mathbf{s}_{\mathbf{t}}^{\mathbf{T}}\mathbf{N}^{\mathbf{H}}}{K_t^2} \tag{20}$$

The matrix $\frac{\mathbf{N}\mathbf{N}^{\mathbf{H}}}{K_t}$ is the interference plus noise estimated covariance matrix whereas $\frac{\mathbf{N}\mathbf{s}_{\mathbf{t}}^{*}\mathbf{s}_{\mathbf{t}}^{\mathbf{T}}\mathbf{N}^{\mathbf{H}}}{K_t^2}$ is the scalar product of interference plus noise vectors with their projection on s_t^*. It follows from (20) that the modified covariance matrix $\mathbf{Q}$ used for MLED in (8) does no longer contain the target contribution and that the target will not be removed contrarily to the clutter by the MLED STAP filter (6). Note that the residual clutter plus noise covariance matrix is slightly different from the actual covariance matrix $\frac{\mathbf{N}\mathbf{N}^{\mathbf{H}}}{K_t}$. It will appear in the simulations that this has no effects on the performance of the APES and the proposed subspace-based APES methods.

If the Doppler cell tested is different from the Doppler cell of the target, $\rho \longrightarrow 0$ and if we make the same approximation than in (12), we have :

$$\mathbf{Q} \approx \mid \alpha \mid^2 \mathbf{s}_{\mathbf{s}}\mathbf{s}_{\mathbf{s}}^{\mathbf{H}} + \frac{\mathbf{N}\mathbf{N}^{\mathbf{H}}}{K_t} - \frac{\mathbf{N}\mathbf{s}_{\mathbf{t}}^{*}\mathbf{s}_{\mathbf{t}}^{\mathbf{T}}\mathbf{N}^{\mathbf{H}}}{K_t^2} \tag{21}$$

When $\rho \neq K_t^2$, the target signal is still in matrix $\mathbf{Q}$, as in $\mathbf{R}$, but this has no effect on the filter because the spatio-temporal steering vector of the Doppler cell $\mathbf{s}_{\mathbf{s}(\mathbf{D})}$ [2]is different from the the spatio-temporal steering vector of the target $\mathbf{s}_{\mathbf{s}(\mathbf{t})}$. We should thus observe a SINR Loss around the Doppler of the target, except at the exact Doppler cell of the target due to the sharpness of the MLED projector [7].

4 Subspace-based APES methods

4.1 APES-EC

The Hung-Turner projection, also called eigencanceller (EC) relies on an eigenvalues decomposition (EVD) of the covariance matrix [12]. This technique is much more robust to a bad estimation of the covariance matrix than the classical Sample Matrix Inversion method [8]. The EC-based STAP filter weight vector is :

$$\mathbf{w} = (\mathbf{Id} - \mathbf{V}_{\mathbf{c}}\mathbf{V}_{\mathbf{c}}^{\mathbf{H}})\mathbf{s}_{\mathbf{s}} \tag{22}$$

where $\mathbf{V_c}$ is the $MN \times p$ dimensional vector containing the orthonormal eigenvectors associated with the p eigenvalues strictly larger than the noise variance. (the noise is supposed Gaussian, i.i.d. and of variance σ^2). The output SINR power is then:

$$\mathbf{P_{ec}} = \frac{|\mathbf{s}_{\mathbf{s}}^{\mathbf{H}}(\mathbf{Id} - \mathbf{V}_{\mathbf{c}}\mathbf{V}_{\mathbf{c}}^{\mathbf{H}})\mathbf{g}|^{\mathbf{2}}}{\mathbf{s}_{\mathbf{s}}^{\mathbf{H}}(\mathbf{Id} - \mathbf{V}_{\mathbf{c}}\mathbf{V}_{\mathbf{c}}^{\mathbf{H}})\mathbf{s}_{\mathbf{s}}} \tag{23}$$

[2]this spatio-temporal steering vector $\mathbf{s_s}$ appearing in (2) is in fact $\mathbf{s_s} = \mathbf{s_1} \otimes \mathbf{s_2}$ where $\mathbf{s_1}$ and $\mathbf{s_2}$ are the purely spatial and purely temporal steering vectors, respectively, and where $\otimes$ is the Kronecker product

When neither targets nor jammers are present, p is the rank of the clutter only covariance matrix. According to Brennan's law [6] :

$$p = M + \beta(N-1) \tag{24}$$

in the case of a uniform linear side-looking antenna [3]. In the case of the presence of J jammers and T targets, there are $p' = p + J + T$ eigenvectors larger than the noise variance while $p' < MN$ and $\mathbf{V_c}$ spans the clutter + jammers + targets subspace.
Without loss of generality, we assume in the following that there are no jammers and only one target is present at the given Doppler cell. The APES-EC filter is deduced from the eigenvalue decomposition (EVD) of matrix $\mathbf{Q}$:

$$\mathbf{Q} = \mathbf{V_Q}\mathbf{\Lambda_Q}\mathbf{V_Q^H} \tag{25}$$

At the Doppler cell of the target, as the target has been removed in $\mathbf{Q}$, the space spanned by the eigenvectors $\mathbf{V_Q}$ is made of the clutter only subspace spanned by $\mathbf{V_c}$ and of the noise subspace spanned by $\mathbf{V_b}$. Let us note :

$$\mathbf{X} = \alpha\mathbf{s_s} + \mathbf{C} + \mathbf{N}' \tag{26}$$

the signal at the Doppler cell of the target . It consists of the target signal, the clutter component $\mathbf{C}$ and the noise only $\mathbf{N}'$. The projector $(\mathbf{Id} - \mathbf{V_c}\mathbf{V_c^H})$ appearing in (22) and applied to $\mathbf{X}$ yields :

$$(\mathbf{Id} - \mathbf{V_c}\mathbf{V_c^H})\mathbf{X} = \alpha\mathbf{s_s} + \mathbf{N}' \tag{27}$$

The clutter has been removed while the first term of the right hand side of (27) has not vanished since $\alpha\mathbf{s_s}$ is not in the dominant clutter only subspace.
At the contrary, since the target is present in $\mathbf{R}$, let us note :

$$\mathbf{R} = \mathbf{V_{c+t}}\mathbf{\Lambda_{c+t}}\mathbf{V_{c+t}^H} + \mathbf{V_b}\mathbf{\Lambda_b}\mathbf{V_b^H} \tag{28}$$

where $\mathbf{V_{c+t}}$ contains the $p+1$ dominant eigenvectors of $\mathbf{R}$ spanning the clutter plus target subspace and where $\mathbf{V_b}$ contains the $MN - p - 1$ eigenvectors spanning the noise only subspace. We can easily deduce that :

$$(\mathbf{Id} - \mathbf{V_{c+t}}\mathbf{V_{c+t}^H})\mathbf{X} = \mathbf{N}' \tag{29}$$

since the target $\alpha\mathbf{s_s}$ is a part of the clutter + target subspace and then since it is orthogonal to the noise subspace. Consequently, at the output of the EC STAP filter, the target has vanished as the clutter and can not be detected contrary to APES.
The subspace methods, like the eigencanceller, are known to only require $2p$ data samples to converge to a $-3dB$ signal loss compared to the $2MN$ samples needed with matrix inversion methods. This detector has however a much higher calculation load than the MLED detector because an EVD of matrix $\mathbf{Q}$ has to be done for each Doppler cell and each range gate. These eigenvalues decompositions have a computational load of about $23(NM)^3$ compared to

[3] $\beta = \frac{2V_a}{\lambda}T_r$ where V_a is the platform velocity, λ is the wavelength and T_r is the pulse repetition interval

the $\frac{16}{3}(NM)^3$ required for a complex matrix inversion [3]. On the contrary, $\mathbf{Q^{-1}}$ can be obtained from $\mathbf{R^{-1}}$ using the Woodbury matrix identity :

$$\mathbf{Q^{-1}} = \mathbf{R^{-1}} + \frac{\mathbf{R^{-1}gg^H R^{-1}}}{\mathbf{1 - g^H R^{-1} g}} \tag{30}$$

This way, only one matrix inversion per range gate has to be done. There is no such technique to find the EVD of the matrix $\mathbf{Q}$ knowing the EVD of matrix $\mathbf{R}$. Thus, the following section will describe a faster method than APES-EC that provides similar performance results with a reduced computational complexity.

4.1.1 APES-FAPI algorithm

In this section, we focus on the Fast Approximated Power Iteration (FAPI) [4] applied to APES. FAPI algorithm builds a base of vectors $\mathbf{W_c}$ that spans the subspace formed by the p dominant eigenvectors given by the EVD of the covariance matrix of a data vector $\mathbf{x_k}$. A brief description of the algorithm that builds $\mathbf{W_c}$ is given in Table 1 (see [4]).
In [5], a range recursive STAP method relying on FAPI has been proposed. In this case, the data vectors $\mathbf{x_k}$ are taken from other range gates of secondary data like in the classical Sample Matrix Inversion method. Here, to apply the APES method with FAPI, we have to remove the signal from the data vector by the following way :

$$\mathbf{Y} = \mathbf{X}(\mathbf{Id}_{K_\mathbf{t}} - \frac{\mathbf{s_t^* s_t^T}}{K_t}) \tag{31}$$

The vector $\mathbf{y_k}$ which is the k^{th} colunm of $\mathbf{Y}$ is used in Table 1 instead of $\mathbf{x_k}$ to compute the vector basis $\mathbf{W}_c$.

Initialisation : $\mathbf{W}_c(0) \leftarrow \mathbf{Id}_{MN*r}, \mathbf{Z}(0) \leftarrow \mathbf{Id}_{p*p}$
FOR $k = 1$ to K_t
$\mathbf{y}(k) = \mathbf{W}_c(k-1)^H \mathbf{x}_k$
$\mathbf{h}(k) = \mathbf{Z}(k-1).\mathbf{y}(k)$
$\mathbf{g}(k) = \frac{\mathbf{h}(k)}{\mathbf{y}^H(k)\mathbf{h}(k)}$
$\mathbf{e}(k) = \mathbf{x}_k - \mathbf{W}(k-1)\mathbf{y}(k)$
$\epsilon^2(k) = \|\mathbf{x}_k^2\| - \|\mathbf{y}_k^2\|$
$\tau(k) = \frac{\epsilon^2}{1+\epsilon^2\|\mathbf{g}(k)\|^2+\sqrt{1+\epsilon^2\|\mathbf{g}(k)\|^2}}$
$\eta(k) = 1 - \tau(k)\|\mathbf{g}(k)\|^2$
$\mathbf{y}'(k) = \eta(k)\mathbf{y}(k) + \tau(k)\mathbf{g}(k)$
$\mathbf{h}'(k) = \mathbf{Z}(k-1)^H \mathbf{y}'(k)$
$\mathbf{d}(k) = \frac{\tau(k)}{\eta(k)}(\mathbf{Z}(k-1)\mathbf{g}(k) - (\mathbf{h}'(k)\mathbf{g}(k))\mathbf{g}(k))$
$\mathbf{Z}(k) = (\mathbf{Z}(k-1) - \mathbf{g}(k)\mathbf{h}'(k)^H + \mathbf{d}(k)\mathbf{g}(k)^H)$
$\mathbf{e}'(k) = \eta(k)\mathbf{x}_k - \mathbf{W}(k-1)y'(k)$
$\mathbf{W}(k) = \mathbf{W}_c(k-1) + \mathbf{e}'(k).\mathbf{g}(k)^H$
ENDFOR

Table 1 : FAPI-APES algorithm

Once $\mathbf{W}_c$ is calculated, the filter's weights can be written like in Equation (22):

$$\mathbf{w} = (\mathbf{Id} - \mathbf{W_c W_c^H})\mathbf{s_s} \tag{32}$$

and the output power is deduced from Equation (23) :

$$\mathbf{P_{FAPI-EC}} = \frac{|\mathbf{s_s^H}(\mathbf{Id} - \mathbf{W_c W^H_c})\mathbf{g}|^\mathbf{2}}{\mathbf{s_s^H}(\mathbf{Id} - \mathbf{W_c W^H_c})\mathbf{s_s}} \tag{33}$$

The computational workload of this method is $o(MNp)$ which is much lower than for the APES-EC or the MLED detector.

5 Performance

Performance results are tested on a simulated side-looking 8 elements ULA antenna. The speed of the platform is $V_a = 100m.s^{-1}$, radar frequency is 10 GHz ($\lambda = 3.10^{-2}m$) and the pulse repetition frequency is set to $\frac{2V_a}{\lambda}$. The radar collects a Coherent Pulse Interval (CPI) of length 64 pulses. Clutter to noise ratio is set to 30 dB and a target of speed $v_t = 28ms^{-1}$ is added into the range gate we focus on. To compare the different methods we will use both the output SNIR power defined in (8), (23), (33), and the SNIR Loss ratio which is defined by :

$$SNIRLoss = \frac{\mathbf{w_q^H R_{th} w_q}}{\mathbf{w^H R w}} \frac{|\mathbf{w^H s}|^\mathbf{2}}{|\mathbf{w_q^H s}|^\mathbf{2}} \tag{34}$$

$\mathbf{w_q}$ is the quiescent weights vector, $\mathbf{R_{th}}$ is the true noise matrix (identity matrix in our case). Note that, by abuse of notation, SNIR Loss are dB-negative values, although they should be postive. For these simulations, we took a pulse window $M = 6$ so that the number of estimates is $K_t = M_p - M + 1 = 59$ for a vector size of $NM = 8 \times 6 = 48$. The line appearing on the output power figures is the threshold for a probability of false alarm of 10^{-6}.

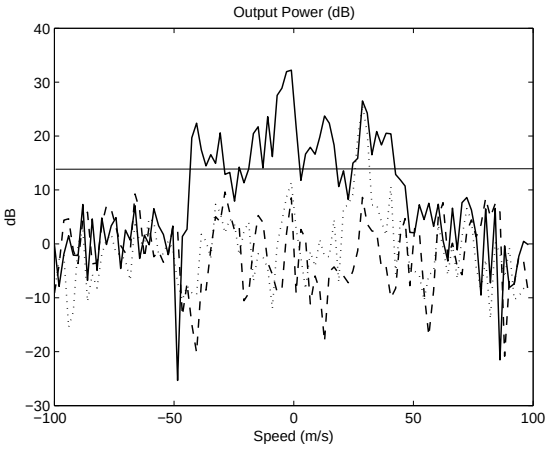

Figure 1: Output SINR power of sum channel (solid curve), optimal filter (dot curve) and classical SMI method (dash curve)

Figures 1 and 2 exhibit the SINR at the output of different STAP filters and as a function of speed (or frequency). The horizontal line indicates the threshold for a probability of false alarm of 10^{-6}. On Figure 1, one can see the SINR at the output of the optimal STAP and for comparison the SINR at the output of the sum channel (no clutter compensation is done) and the SINR at the output of the classical SMI (the clutter is removed but the target is also eliminated).

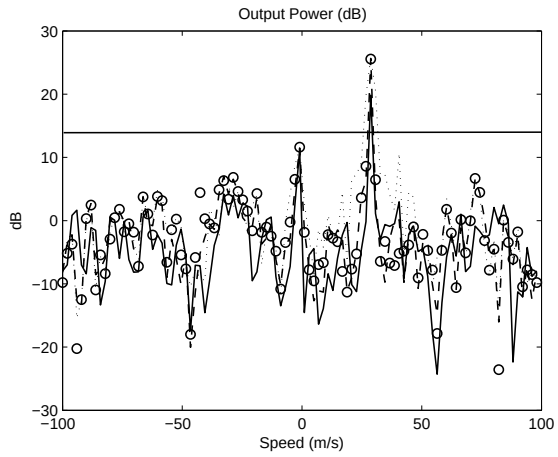

Figure 2: Output SINR power of MLED (solid curve), optimal filter (dot curve), APES-EC (dash curve) and FAPI-APES (circles)

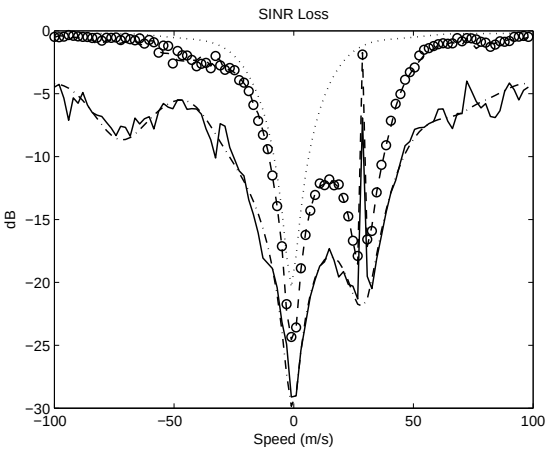

Figure 4: SINR Loss of optimal filter (dot curve), APES-EC (dash curve), FAPI-APES (circles), MLED (solid curve) and classical SMI method (dash-dot curve)

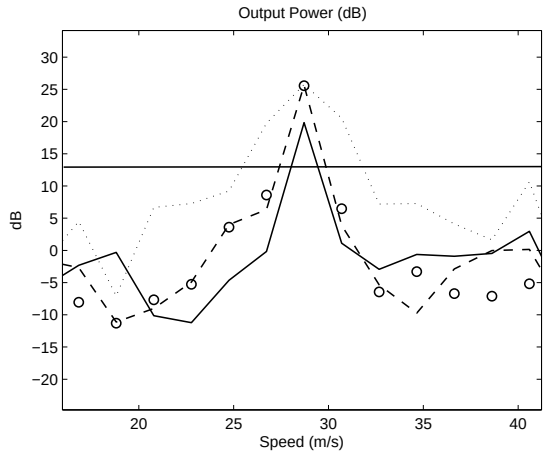

Figure 3: Zoom on output SINR power of optimal filter (dot curve), MLED detector (solid curve), FAPI-APES (circles) and APES-EC (dash curve)

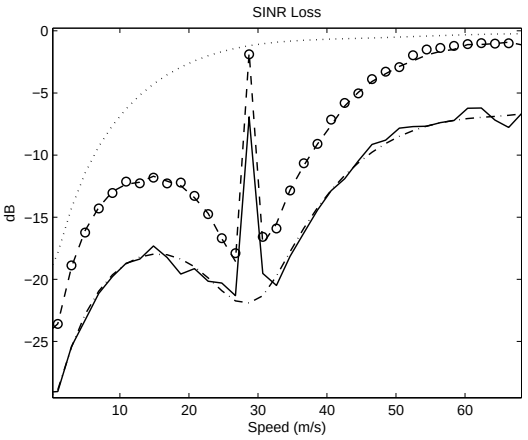

Figure 5: Zoom on SINR Loss of optimal filter (dot curve), APES-EC (dash curve), FAPI-APES (circles), MLED (solid curve) and classical SMI method (dash-dot curve)

The SINR performance at the output of the MLED, APES-EC, FAPI-APES and optimal STAP is plotted on Figure 2. One can see that the APES type algorithms succeeded to reject the clutter without eliminating the target. Figure 3 is a zoom of Figure 2 around the target. This is to show that the subspace-based APES-EC and FAPI-APES outperform APES with a gain of at least 5 dB. Also note that APES-EC and FAPI-APES give similar results whereas FAPI-APES is much less computationally complex than APES-EC.
Figure 4 exhibits the SNIR Loss as a function of speed for the optimal , SMI, MLED, APES-EC and APES-FAPI STAP filters. One can see that since the number of snapshots used for the estimation of the covariance matrix in (3) is less than $2MN$, the SNIR Loss for SMI and MLED is about 6 dB less than the optimal STAP even in the exoclutter and exo-target speeds regions. The MLED, however, allows not to reject the target while SMI does not. This figure shows that APES-EC and FAPI-APES not only keep the target out of the clutter but also allow a SNIR Loss very close to the optimal one in the exo-clutter and exo-target areas. Figure 5 is a zoom of Figure 4 around the target speed. One can see the gain of the proposed APES-EC and FAPI-APES over the MLED on the SINR Loss at the target speed.

6 Conclusion

In this paper, we propose a more robust version of the MLED algorithm based on subspace methods. This enables the STAP processing to require less data for estimation, which is often needed in heterogeneous situations, while keeping good performances. Our new FAPI-APES algorithm has the same performances as APES-EC, and it also reduces significantly the workload of the APES-EC, even surpassing the MLED detector in computational complexity.

Acknowledgements

The authors would like to thank the DGA from the French Ministry of Defense for their support.

References

[1] E. Aboutanios and B. Mulgrew. A stap algorithm for radar target detection in heterogeneous environments. In *Statistical Signal Processing, 2005 IEEE/SP 13th Workshop on*.

[2] E. Aboutanios and B. Mulgrew. Evaluation of the single and two data set stap detection algorithms using measured data. *2007 IEEE International Geoscience and Remote Sensing Symposium*, pages 494–498, 2007.

[3] M Arakawa. Computational workloads for commonly used signal processing kernels. *Lincoln Laboratory*, 2006.

[4] R. Badeau, B. David, and G. Richard. Fast approximated power iteration subspace tracking. *Signal Processing, IEEE Transactions on*, 53(8):2931 – 2941, aug. 2005.

[5] S. Beau and S. Marcos. Range dependent clutter rejection using range-recursive space-time adaptive processing (stap) algorithms. *Signal Processing*, 90(1):57–68, 2010.

[6] L.E. Brennan and I.S. Reed. Theory of adaptive radar. *IEEE Transactions On Aerospace And Electronic Systems*, AES-9(2):237–252, 1973.

[7] J.-F. Degurse, L. Savy, R. Perenon, and S. Marcos. An extended formulation of the maximum likelihood estimation algorithm. application to space-time adaptive processing. In *Radar Symposium (IRS), 2011 Proceedings International*, pages 763 –768, sept. 2011.

[8] A. Haimovich. The eigencanceler: adaptive radar by eigenanalysis methods. *IEEE Transactions on Aerospace and Electronic Systems*, 1996.

[9] R. Klemm. *Principles of space-time adaptive processing*. The Institution of Electrical Engineers (IEE), 2002.

[10] W.L. Melvin. A stap overview. *IEEE Aerospace And Electronic Systems Magazine*, 19(1):19–35, 2004.

[11] Li H. Stoica P. and J Li. A new derivation of the apes filter. *IEEE Signal Processing Letters*, pages 205–206, 1999.

[12] M. Zatman. Properties of hung-turner projections and their relationship to the eigencanceller. In *Signals, Systems and Computers, 1996. Conference Record of the 30th Asilomar Conference on*.